313

A Fractal Approach to Model Soil Structure and to Calculate Thermal Conductivity of Soils

P. LEHMANN*, M. STÄHLI, A. PAPRITZ, A. GYGI and H. FLÜHLER
Institute of Terrestrial Ecology, Soil Physics, Swiss Federal Institute of Technology, ETH Zürich, Grabenstrasse 3, 8952 Schlieren, Switzerland

Abstract. Heat transport in soils depends on the spatial arrangement of solids, ice, air and water. In this study, we present a modified fractal approach to model the pore structure of soils and to describe its influence on the thermal conductivity. Three different fractal generators were sequentially applied to characterize a wide range of particle- and pore-size distributions. The given porosity and particle-size distribution of a clay, clay loam, silt loam and loamy sand were successfully modeled. The thermal conductivity of the fractal soil model was calculated using a network of resistors. We applied a renormalization approach to include the effects of smaller scale structures. The predictions were compared with the empirical Johansen' model (Johansen, 1975), that postulates a simple linear relationship between ice content and thermal conductivity. For high ice-saturated conditions, the calculated thermal conductivity agrees well with the empirical model. To describe partial ice saturation, we assumed that some pores were coated by ice films enclosing the air-filled center. In addition, we introduced a reduced heat exchange coefficient of the particles for unsaturated conditions. The ice-saturated and -unsaturated thermal conductivity calculated with this approach was very similar to that estimated by the empirical model. The variation of the thermal conductivities for different spatial arrangements of pores and particles in the prefractals were determined. Extreme values deviate more than 50% from the mean values.

Key words: pore–solid-fractals, prefractals, soil texture, thermal conductivity, upscaling, spatial arrangement.

1. Introduction

In this study, we postulate a three-dimensional fractal model that mimics the structure of different soils. From the structural model, we obtain the thermal conductivity of the soil. Heat transfer in soils is of crucial importance for the living conditions of soil organisms, for the physical state of soil water and for the mechanical stability of permafrost soils.

All constituents of a soil conduct heat. While the thermal conductivities of solids and ice-filled pores are high, it is lower in water-filled pores and extremely small in air-filled pores. The thermal conductivity of soils depends on the mass and volume fraction of the various soil constituents and on their spatial arrangement.

---

*Author for correspondence: e-mail: lehmann@ito.umnw.ethz.ch

The configurations with the solid and air phase arranged in parallel (maximum conductivity) or in series (minimum conductivity) represent the extremes of thermal conductivity for a soil with given porosity. In the past, several approaches have been proposed to predict the thermal conductivity for a given mass and volume fraction of soil constituents. Smith (1942) assumed a parallel arrangement of air-filled pores and particles separated by air gaps. Similarly, Mickley (1951) described a parallel arrangement of air, solid phase and elements containing both phases. Hashin and Shtrikman (1962) and Miller (1969) determined the range of thermal conductivity values for heterogeneous materials by means of perturbation analysis. They included shape and thermal conductivity of the components and the porosity of the material. However, the determined range was much too wide to be used for predicting the thermal conductivity of soils. Without additional information about pore- and particle-size distribution and the arrangement of ice, liquid water, air and solids, the thermal conductivity of soils cannot be obtained correctly. Mohanty (1997) did some work along these lines by calculating the multiphase heat flow through sandstone and soil samples based on a structural analysis of thin sections of these porous materials. Such measurements are time consuming and cannot be routinely carried out. In addition, using a single measuring method will give us detailed information at only one scale, and we shall still lack data about the role of soil structures at smaller and larger scales.

In this study, we introduce a fractal approach to obtain a realistic model of soil structure. The model accounts for the spatial arrangement of pores and solid elements with a wide range of sizes. In a fractal geometry, the same structure occurs at any spatial resolution. Of course, the mathematical concept of self-similarity for infinitely small scales is not valid and must be restricted to a certain range of scales.

The fractal approach has the advantage that it describes a multiscale structure with a single parameter, namely the *fractal dimension*. Tyler and Wheatcraft (1990) calculated the water retention function of capillary bundles with fractal cross-sections and they showed that the resulting water retention characteristic is equivalent to the Brooks and Corey (1964) model. Rieu and Sposito (1991) described pore- and aggregate-size distributions of three-dimensional fractal structures for a finite number of iterations. Both of these approaches fail to describe pore-size distributions that cannot be characterized by a single power-law and they also fail for simultaneously generating the pore- *and* particle-size distribution. Bird *et al*. (1996) obtained wider pore-size distributions by using two different scaling factors. Similarly, Perfect *et al*. (1993) used a multifractal approach to model different aggregate- and particle-size distributions, where the fragmentation process depends on the scale of the elements. In both cases, only pore- *or* particle-size distributions were modeled. Recently, Perrier *et al*. (1999) presented the pore–solid-fractal (PSF) approach, which simultaneously models the size distributions of pores *and* particles. The resulting power-law characterizes narrow particle- and pore-size distributions but fails to describe broad size distributions.

In this study, we extend the PSF of Perrier *et al.* (1999) by combining three fractal processes in series. The resulting three-generator-pore–solid-fractal (3G-PSF) approach accounts for a wide range of particle- and pore-size distributions. We then show that 3G-PSF can be successfully used to predict the thermal conductivity, a soil property which depends not only on the mass and volume fractions but also on the spatial arrangement of the soil constituents. In this paper, we describe both fractal approaches (PSF, 3G-PSF) and give the equations to model the pore- and particle-size distributions and the bulk volume (or mass) fractions of the phases. Then, we use the two approaches to model the porosity and particle-size distributions of four different soils with contrasting texture and demonstrate the suitability of the 3G-PSF approach.

Based on this structural concept, we calculate the thermal conductivity of fractal structures using a network model. We compute the thermal conductivities of the four soil materials for different air contents and compare the results with an empirical model widely used to characterize thermal properties of soils.

2. Fractal Models of Soil Structure

2.1. PORE–SOLID-FRACTALS, PSF

First, we summarize some characteristics of the PSF approach as proposed by Perrier *et al.* (1999). The generation of a PSF starts with the *initiator*, a cube of length L. This initial cube is divided into R^3 subcubes with length LR^{-1}. The number of subcubes representing pores is denoted by P, the number of subcubes representing particles is S (solids) and the remaining $F = R^3 - S - P$ subcubes will be specified in the next iteration step. The structure specified by the *scaling factor R*, the number of pores P and particles S is called the *generator*. At each scale, the same generator is applied to characterize yet unspecified subcubes. The structure generated after n iterations is referred to as a *prefractal* of order n. We can distinguish different *configurations* of a generator (and a prefractal), characterized by the same numbers R, P and S, but with different spatial arrangements of the R^3 elements. The number of unspecified elements $F = R^3 - P - S$ can be used to define the *fractal dimension $D_{\text{fractal}} = \log F / \log R$* (Mandelbrot, 1982).

In Figure 1(b), a PSF with $R = 3$, $P = 7$ and $S = 8$ is compared with the well known Menger sponge (Figure 1(a)) with $R = 3$, $P = 7$ and $S = 0$. Both illustrations show prefractals of order three. After three iterations, all the subcubes of the Menger sponge not yet specified as pores, may be interpreted as particles of uniform size LR^{-3}. However, the solid phase vanishes for infinitely many iterations and a structure with dust-like solids and a porosity of $1.0\,\text{m}^3\,\text{m}^{-3}$ results.

The distribution of particle- and pore-sizes, generated by the PSF-model, are power-laws, and they are completely specified by R, P and S. In iteration $1 \leqslant i < n$ the number of subcubes assigned to be pores or particles is equal to $F^{i-1}P$ and $F^{i-1}S$, respectively. The respective volumes, p_i and s_i, are equal to $F^{i-1}PL^3R^{-3i}$, and $F^{i-1}SL^3R^{-3i}$. In iteration $i + 1$ a smaller volume of pores (or solids) is
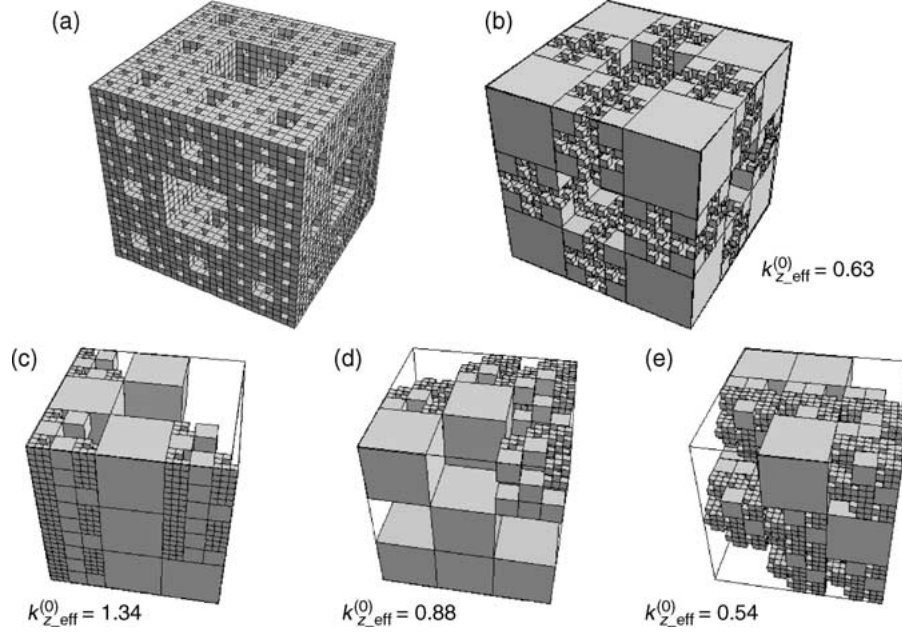
Figure 1. Prefractals of order $n = 3$ for the Menger-sponge (a) and a PSF (b). Other configurations of the PSF constructed with a generator containing $S = 8$ particles and $P = 7$ pores are shown (c–e). The thermal conductivities of the PSF prefractals of order $n = 10$ are given. All elements not assigned to be pores after three iterations are shown.

generated than in iteration i because

$$\frac{p_{i+1}}{p_i} = \frac{PF^i(L/R^{i+1})^3}{PF^{i-1}(L/R^i)^3} = \frac{s_{i+1}}{s_i} = \frac{SF^i(L/R^{i+1})^3}{SF^{i-1}(L/R^i)^3} = \frac{F}{R^3} < 1.$$

Thus, the volume fractions of pores and particles of size LR^{-i} decrease monotonically with i.

For a prefractal of order n, the particle- and pore-size distributions and the derived quantities porosity ϕ_n (volume of pores per total volume) and bulk density $\rho_{\text{bulk},n}$ (mass of solids per total volume) can be expressed as geometrical series. We assume that the density of the particles ρ_{particle} does not depend on their size and that all the subcubes generated in the very last iteration, excluding those that are explicitly assigned to be pores, are considered as particles. This means, that s_n, the volume of particles generated in the last iteration n, is equal to $F^{n-1}(S+F)L^3R^{-3n}$. Then, we find for prefractals of order n

$$\phi_n = \frac{1}{L^3} \sum_{i=1}^{i=n} p_i = \frac{P}{R^3}\left(\frac{1 - (F/R^3)^n}{1 - (F/R^3)}\right) = \left(\frac{P}{P+S}\right)\left(1 - \left(\frac{F}{R^3}\right)^n\right),$$

$$\frac{\rho_{\text{bulk},n}}{\rho_{\text{particle}}} = \frac{1}{L^3}\left(s_n + \sum_{i=1}^{i=n-1} s_i\right) = \frac{S + P(F/R^3)^n}{S + P}.$$

In the limit $n \to \infty$ this yields

$$\phi_\infty = \frac{P}{P + S},$$

$$\frac{\rho_{\text{bulk},\infty}}{\rho_{\text{particle}}} = \frac{S}{P + S}.$$

For a prefractal of order n, the cumulative volume fraction of pores with size $r < LR^{-i}$, is equal to

$$\frac{\sum_{j=i+1}^{j=n} p_j}{\sum_{j=1}^{j=n} p_j} = \frac{\sum_{j=1}^{j=n} p_j - \sum_{j=1}^{j=i} p_j}{\sum_{j=1}^{j=n} p_j} = \frac{\phi_n - \phi_i}{\phi_n} = \frac{(F/R^3)^i - (F/R^3)^n}{1 - (F/R^3)^n},$$

and the corresponding fraction for particles is

$$\frac{\sum_{j=i+1}^{j=n} s_j}{\sum_{j=1}^{j=n} s_j} = \frac{\sum_{j=1}^{j=n} s_j - \sum_{j=1}^{j=i} s_j}{\sum_{j=1}^{j=n} s_j} = \frac{\rho_{\text{bulk},n} - \rho_{\text{bulk},i}}{\rho_{\text{bulk},n}}$$

$$= \frac{P(F/R^3)^n + S(F/R^3)^i}{P(F/R^3)^n + S}.$$

In the limit $n \to \infty$ we obtain

$$\frac{\phi_\infty - \phi_i}{\phi_\infty} = \frac{\rho_{\text{bulk},\infty} - \rho_{\text{bulk},i}}{\rho_{\text{bulk},\infty}} = \left(\frac{F}{R^3} \right)^i. \tag{1}$$

2.2. PORE–SOLID-FRACTALS WITH THREE GENERATORS, 3G-PSF

It is obvious that the PSF-model suffers from two deficiencies. First, it is valid only for soils with the largest particles and pores being the most abundant. This may hold for many sands, but certainly not for soils in general. Second, the cumulative distributions of pore- and particle-sizes (Equation (1)) are power-laws which appear as straight lines when plotted on a log–log scale

$$\log \left(\frac{\rho_{\text{bulk},\infty} - \rho_{\text{bulk},i}}{\rho_{\text{bulk},\infty}} \right) = (D_{\text{fractal}} - 3) \log \, L + (3 - D_{\text{fractal}}) \log \, r_i,$$

with size $r_i = LR^{-i}$. Recently, Bittelli *et al.* (1999) showed that such a single power-law relation between cumulative mass and size of soil particles cannot characterize measured particle-size distributions of soils. They concluded that a combination of three different power-laws, each valid for a certain range of particle-sizes, is required to describe observed size distributions satisfactorily. Based on this idea, we built a PSF-model using three different generators, each applied for a certain number of iterations, only. To illustrate the following formal description
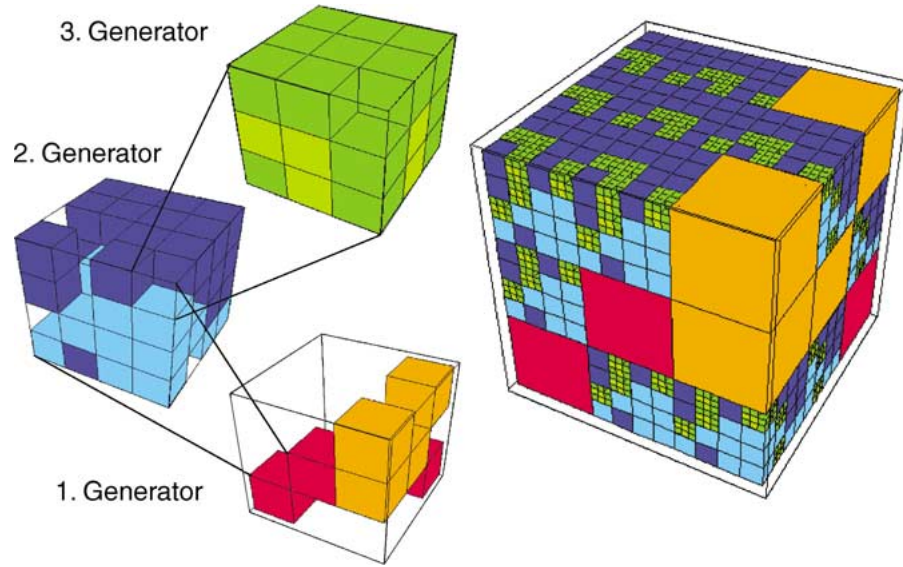
Figure 2. Construction of a PSF with three generators. Particles are drawn in dark and pores in bright colors. The resulting prefractal is of order $n = 3$. The scale factor is $R = 4$ for the second and $R = 3$ for the first and third generator.

of the procedure, Figure 2 shows a prefractal of order three obtained by applying three different generators only once.

We start again with a cube of length L. A first generator, characterized by the integers R_1, P_1 and S_1, is applied to the initial cube and divides it into R_1^3 subcubes of length LR_1^{-1}. The set of P_1 subcubes are assigned to be pores, S_1 subcubes to be solids, and $F_1 = R_1^3 - P_1 - S_1$ subcubes will be subjected to further steps of the generator. After n_1 iterations, $F_1^{n_1}$ subcubes with length $LR_1^{-n_1}$ are neither pores nor solid particles. These subcubes are subdivided by a second generator, characterized by R_2, P_2 and S_2. After the first application of the second generator, $F_1^{n_1} P_2$ pores with length $LR_2^{-1}R_1^{-n_1}$ are obtained. Finally, after n_2 iterations of the second generator, a third generator, specified by R_3, P_3 and S_3 is used for the remaining $F_1^{n_1} F_2^{n_2}$ cubes with length $LR_2^{-n_2}R_1^{-n_1}$, that were not yet assigned to be pores or particles. For the very last iteration, all subcubes not explicitly denoted as pores are assigned to be particles. After n_3 iterations of the third generator, the following expressions for the bulk density and the porosity are found

$$
\begin{aligned}
\phi_{(n_1+n_2+n_3)} &= \frac{P_1}{P_1 + S_1}\left(1 - \left(\frac{F_1}{R_1^3}\right)^{n_1}\right) \\
&+ \left(\frac{F_1}{R_1^3}\right)^{n_1} \frac{P_2}{P_2 + S_2}\left(1 - \left(\frac{F_2}{R_2^3}\right)^{n_2}\right) \\
&+ \left(\frac{F_1}{R_1^3}\right)^{n_1}\left(\frac{F_2}{R_2^3}\right)^{n_2} \frac{P_3}{P_3 + S_3}\left(1 - \left[\left(\frac{F_3}{R_3^3}\right)^{n_3}\right]\right),
\end{aligned}
$$

$$\frac{\rho_{\text{bulk},(n_1+n_2+n_3)}}{\rho_{\text{particle}}} = \frac{S_1}{P_1 + S_1}\left(1 - \left(\frac{F_1}{R_1^3}\right)^{n_1}\right)$$
$$+ \left(\frac{F_1}{R_1^3}\right)^{n_1}\frac{S_2}{P_2 + S_2}\left(1 - \left(\frac{F_2}{R_2^3}\right)^{n_2}\right)$$
$$+ \left(\frac{F_1}{R_1^3}\right)^{n_1}\left(\frac{F_2}{R_2^3}\right)^{n_2}\frac{S_3 + [P_3(F_3/R_3^3)^{n_3}]}{P_3 + S_3}.$$

Note, that only the terms in brackets vanish for $n_3 \to \infty$. Now, pore- and particle-size distributions are no longer necessarily monotonically decreasing, because in iteration $n_1 + 1$, the first iteration with the second generator, more pore volume (or particle mass) may be generated than in iteration n_1

$$\frac{p_{n_1+1}}{p_{n_1}} = \frac{(P_2/R_2^3)(F_1/R_1^3)^{n_1}}{(P_1/R_1^3)(F_1/R_1^3)^{n_1-1}} = \frac{P_2 F_1}{P_1 R_2^3}$$
$$\frac{s_{n_1+1}}{s_{n_1}} = \frac{(S_2/R_2^3)(F_1/R_1^3)^{n_1}}{(S_1/R_1^3)(F_1/R_1^3)^{n_1-1}} = \frac{S_2 F_1}{S_1 R_2^3}.$$

In case of a first generator with small P_1 (or S_1) and large F_1 and a second generator with large P_2 (or S_2) this ratio will be larger than one. This corresponds to a pore- (or particle-) size distribution with two maxima. Analogously, a third maximum is possible when changing from the second to the third generator.

Since we apply three different generators, each defined by a characteristic fractal dimension, the reader might think that our approach is related to the concept of multifractals. Whereas three fractal dimensions define a 3G-PSF, a multifractal is characterized by a continuous distribution of fractal dimensions. Following Perfect *et al.* (1993), the fractal dimension of a multifractal changes with the number of iterations, that is, with the spatial scale, according to a function containing an exponential term. For a 3G-PSF fractal, the fractal dimension changes only at two scales, and the scales where the changes occur can be chosen arbitrarily. The description of a multifractal given by Perfect *et al.* is a special case of multifractals, also denoted as multiscale fractal. With a more general definition, multifractals cannot be characterized by a single fractal dimension, but must be represented by fractal subsets having different scaling exponents (Feder, 1988). Sahimi (1995) gives the following illustration of a multifractal: if a multifractal is broken into many pieces, each piece can be described by a fractal dimension, and these fractal dimensions can be different. With this (more general) description, the fractal dimension of a multifractal is not scale dependent. So, from this point of view, the 3G-PSF approach is not related to the concept of multifractality.

3. Fractal Models of Different Soil Materials

To compare the single generator PSF with the extended 3G-PSF fractal approach, we chose four soil materials with different textures. We used simulated data, that

are characteristic for a loamy sand, a silt loam, a clay loam and a clay. For these soils, the mass fractions of the following particle size classes (in μm) were given: [1000–250], [250–100], [100–65], [65–25], [25–10], [10–2] and [2–0]. The porosity of all these soils was equal to $0.40\,\mathrm{m}^3\,\mathrm{m}^{-3}$.

To compare these values with the mass fractions simulated by the PSF approaches, we obeyed the following recipe: the particles generated in iteration i have the diameter LR^{-i}. All these particles are larger than $LR^{-(i+1)}$. So, we allocate the mass generated in iteration i to the size class with particles with diameter ranging from $LR^{-(i+1)}$ to LR^{-i}. If this two values belong to two different soil particle-size classes, we allocated the simulated mass to the two classes proportional to the length of the overlaps on a log-length scale.

In the next two subsections, we explain the fitting procedure. We will optimize four (single generator PSF) and nine (3G-PSF) parameters, respectively, to fit the porosity (one value) and the particle-size distribution (seven values). We do not use a gradient based fitting algorithm that eventually would lead to a system of linear equations. Such a procedure would result in an under-determined system for the 3G-PSF model. Instead, we perform a grid search in the parameter space to find the optimal parameter set.

3.1. FITTING PORE–SOLID-FRACTALS WITH SINGLE GENERATOR (PSF)

We shall now present the results obtained by fitting a single generator PSF to the observed particle-size distributions. For this model, the size of the initiator L, the number of particles, S, and of pores, P, was optimized. The number of iterations n was restricted by the condition $LR^{-n} < 2\,\mu$m. The scaling factor remained fixed at $R = 3$ in all instances. The parameter space considered for S and P was the set $[0, 1, \ldots, 27]$, and for L we used the set $(50\,\mu\mathrm{m} + k \cdot 5\,\mu\mathrm{m}, k = 1, 2, \ldots, 590)$. Subject to the constraint that the simulated porosity had to deviate less than $0.01\,\mathrm{m}^3\,\mathrm{m}^{-3}$ from the given porosity, we selected the set of parameters that minimized the sum of absolute deviations between simulated and observed mass fractions by complete enumeration.

The results obtained by fitting the PSF to the particle-size data are summarized in Table I and in Figure 3. The best agreement between simulation and data was found for the loamy sand. Sandy soils often have unimodal particle-size distributions with a large mode and they can be described well by a single power-law. The poorest agreement was found for the clay. In case of clay, a considerable amount of larger particles was observed. This fraction was not generated with a single generator approach.

3.2. FITTING PORE–SOLID-FRACTALS WITH THREE GENERATORS (3G-PSF)

We now present the results obtained for the 3G-PSF. For this model, nine parameters were optimized. The size of the initiator L, the number of iterations with

Table I. Parameters of PSF and 3G-PSF fitted to particle-sizes and porosities of four soils with contrasting texture. The error denotes the mass fraction of modeled particles assigned to a wrong particle-size class

Soil type		$L[\mu m]$	P_1	S_1	n_1	P_2	S_2	n_2	P_3	S_3	n_3	Error %
Clay												
	3G-PSF	1180	4	1	3	2	0	1	0	2	2	3.94
	PSF	55	4	3	4	–	–	–	–	–	–	50.75
Clay loam												
	3G-PSF	1360	2	3	1	3	3	2	4	4	3	2.44
	PSF	1070	4	5	6	–	–	–	–	–	–	34.18
Silt loam												
	3G-PSF	520	2	3	2	9	12	1	3	3	3	9.97
	PSF	120	6	8	4	–	–	–	–	–	–	30.00
Loamy sand												
	3G-PSF	1580	5	9	2	10	6	2	2	0	3	2.58
	PSF	1590	6	9	7	–	–	–	–	–	–	10.54

the first and second generator, n_1 and n_2, and the number of solids and pores, S_1, P_1, S_2, P_2, S_3 and P_3 of the three generators were optimized. For the total number of iterations, the condition $LR^{-(n_1+n_2+n_3)} < 2\,\mu m$ had to be fulfilled.
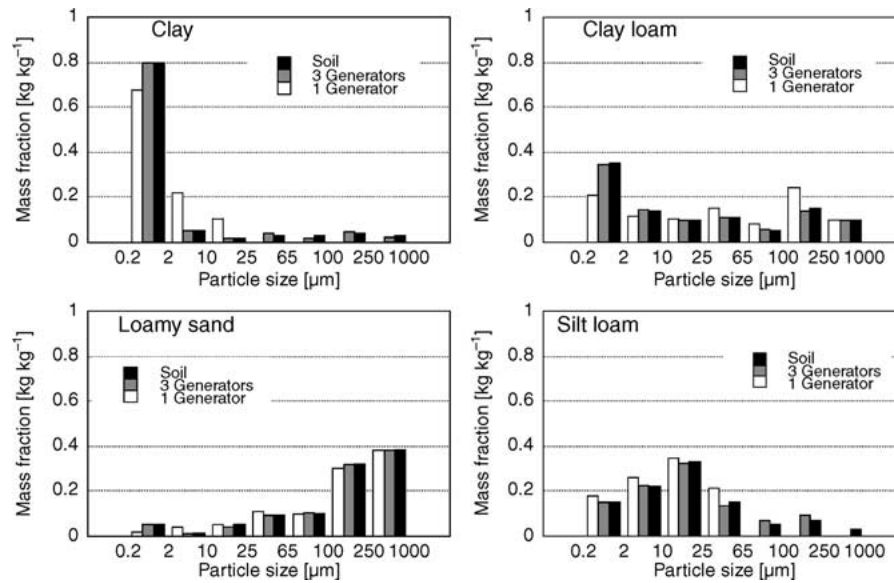

Figure 3. Comparison between the observed and fitted particle-size distribution of four soils. Simulations were carried out with one and three generators.

The scaling factor was set $R = 3$. Since it was no longer feasible to compute the problem for all the possible parameter combinations, we used a two step procedure to fit the model. First, we used a coarse discretization of the parameter space to find 'optimized initial values' to be used for a refined local search in the subsequent second step. The parameter space considered in the first step was the set $[0, 3, \ldots, 27]$ for the number of particles and pores of the three generators and the set $[200, 400, \ldots, 2000\,\mu\text{m}]$ for the initiator L. We imposed the constraint, that each generator had to be applied at least once and that the modeled porosity had to deviate less than $0.01\,\text{m}^3\,\text{m}^{-3}$ from the observed value. Denoting the optimized initial values by L^*, S_k^* and P_k^*, $k = 1, 2, 3$, the parameter space considered in the second step of the fitting procedure was given by all the combinations of the values $[L^* - 200, L^* - 180, \ldots, L^* + 200\,\mu\text{m}]$, $[P_k^* - 3, P_k^* - 2, \ldots, P_k^* + 3]$ and $[S_k^* - 3, S_k^* - 2, \ldots, S_k^* + 3]$, with $k = 1, 2, 3$ that satisfied the imposed constraints. For n_1 and n_2, the same range of values was considered as in the first step. The 3G-PSF modeled the observed particle size distributions quite well (Table I and Figure 3). The maximum difference between simulated and observed mass fractions was less than 10% for all soils. The largest error was found for the silt loam where the model predicted zero mass for the size class 250–1000 μm. The good agreement between model predictions and data confirms the results of Bittelli *et al*. (1999), who found that a combination of three power-law distributions are adequate to characterize any particle-size distribution.

Not withstanding the success of the 3G-PSF in modeling the size distribution of the phases, we shall now explore whether the approach is similarly successful in describing thermal conductivity, a soil property that depends not only on the volume and mass fractions but also on the spatial arrangement of the soil constituents.

4. Thermal Conductivity of Fractal Geometries

The description of heat conductance is analogous to that of electrical conductivity. A review of electrical conductivity through disordered systems and fractals is given by Clerc *et al*. (1990). Adler (1992) calculated water conduction and other transport processes through fractal geometries, while Thovert *et al*. (1990) investigated the thermal conductivity of fractals. In this study, we will quantify the heat conductance through PSF.

4.1. THERMAL CONDUCTIVITY OF A COMPOSITE STRUCTURE

The heat flux I_{heat} [kg m^2 s^{-3}], the flow of heat energy ΔQ_{heat} [kg m^2 s^{-2}] per time Δt through a conductor of cross section A [m^2] and length Δx [m] driven by a temperature difference ΔT [K], is proportional to the thermal conductivity k [kg m s^{-3} K^{-1}] of the conductor

$$I_{\text{heat}} = \frac{\Delta Q_{\text{heat}}}{\Delta t} = -kA\frac{\Delta T}{\Delta x}. \tag{2}$$

The thermal conductivity k corresponds to an inverse specific resistance ξ

$$|k| \equiv \left| \frac{1}{\xi} \right|,$$

where ξ denotes the resistance of a cube with length 1 m.

Thus, we can define a heat resistance network and calculate the heat flow I_{heat} through composite structures using Kirchhoff's laws. In the next subsection, we will calculate at each scale the effective thermal conductivity of a composite structure consisting R^3 elements. We assume that these elements all have side length of 1 m, so that their resistance is equal to the specific resistance ξ. We calculate the heat flow through the structure assuming a temperature difference ΔT between bottom and top and no-heat-flow in the xz- and yz-planes bounding the structure. Thus, heat exchange is allowed in x-, y-, and z-direction between adjacent elements and in z-direction for heat transfer across the bounding bottom and top planes of the structure. In total, $(3R - 1)R^2$ heat flow components between connected elements and between surface elements and their environment must be quantified. In Figure 4(e) the 20 components for a structure with $R = 2$ are enumerated. We used Kirchhoff's law to formulate the equations that relate heat flow, temperature gradient and resistance, and we solved the system numerically. For $R = 3$, as an
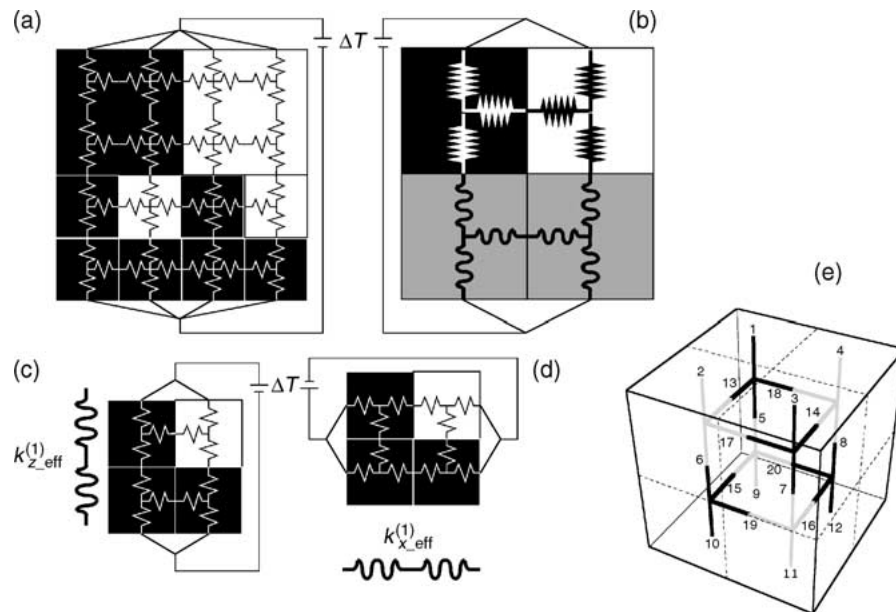

Figure 4. Schematic explanation of the procedure used to upscale thermal conductivity. Each zigzag-line indicates a heat conductor. The network containing 32 flow components (a) is replaced by an upscaled network with only eight components (b). To calculate the conductance of the gray composite elements, a temperature gradient is applied in the x- and z-direction, respectively (c, d). The enumeration of the heat flow components is shown for a structure containing eight elements (e).

example, we have to solve 72 equations. Given the solution for the network flow problem, we can then compute the total flow of heat across the structure and from Equation (2) we immediately find its effective conductivity $k_{\text{eff}} = I_{\text{heat}} \Delta T^{-1} R^{-1}$.

4.2. UPSCALING THERMAL CONDUCTIVITY

To find the effective conductivity of a prefractal of order n, containing R^{3n} elements, all the flows associated with a network of $R^{2n}(3R^n - 1)$ components must be calculated. Table I shows that the 3G-PSF prefractals fitted to the particle-size distribution of the four soil materials were of orders 6 and 7. For each configuration of a prefractal of this order, one or three billions of equations must be solved which, by far, exceeds available computing resources. Hence, efficient approximation methods to upscale thermal conductivity are required. Our upscaling procedure is similar to the two-dimensional approach presented by Gautier and Noetinger (1997). Since for three dimensions the resulting set of equations is rather intricate, we derive it in some detail.

4.2.1. *Final Iteration*

We start with the analysis of the finest composite structures, containing P pores and $R^3 - P$ particles of size LR^{-n} determined in the last iteration. We solve the flow problem for such a composite structure using Kirchhoff's law and get its effective thermal conductivity. The heat flow through the composite element and hence its effective conductivity depends on the applied boundary conditions. For a temperature gradient applied in z-direction and no-flow conditions at the bounding xz- and yz-planes, we denote the obtained conductivity as $k_{z\_\text{eff}}^{(n-1)}$. Similarly, for a temperature gradient applied in y-direction and no-flow conditions through the xy- and yz-planes, we obtain $k_{y\_\text{eff}}^{(n-1)}$, and finally, for a temperature gradient applied in x-direction and no-flow conditions through the xy- and xz-planes, the effective conductivity is $k_{x\_\text{eff}}^{(n-1)}$. By using the notation $k^{(n-1)}$ we explicitly indicate the size of the composite structure, namely $LR^{-(n-1)}$, containing R^3 elements of size LR^{-n}.

4.2.2. *First Step of Upscaling*

Next, we solve the heat flow problem for the structures generated in iteration $n - 1$ containing P pores, S particles and $F = R^3 - S - P$ composite elements. The thermal properties of the R^3 elements are characterized by k_{pore} for pores, k_{particle} for particles and $k_{z\_\text{eff}}^{(n-1)}$, $k_{y\_\text{eff}}^{(n-1)}$, $k_{x\_\text{eff}}^{(n-1)}$ for the F composite elements. The solution of the flow problem at this scale yields $k_{z\_\text{eff}}^{(n-2)}$, $k_{y\_\text{eff}}^{(n-2)}$, $k_{x\_\text{eff}}^{(n-2)}$, the effective conductivities of the composite structure of size $LR^{-(n-2)}$. To illustrate this procedure, an example is given in Figure 4 for a two-dimensional prefractal of order two, containing one large particle, six small particles, one large and two small pores. A temperature gradient is applied in the z-direction. To determine the effective conductivity of the structure, we have to solve the heat flow through

a resistance network containing 20 vertical and 12 horizontal heat flow components (Figure 4(a)). We simplify the problem by considering six vertical and two horizontal components (Figure 4(b)). To approximate the resistances through the composite elements (gray squares), we calculated the effective conductivities $k^{(1)}_{z\_\text{eff}}$ and $k^{(1)}_{x\_\text{eff}}$ for temperature gradients applied in z- and x-direction, respectively (Figure 4(c) and (d)).

4.2.3. *Comparison of Upscaling with Direct Solution*

For a three-dimensional prefractal of order 2, the quality of this approximation is shown in Figure 5. To this end, we used the generator $R = 3$, $S = 9$, $P = 9$ and obtained, after the second iteration, FP pores and $F(S + F)$ particles of size LR^{-2}. First, we represented the prefractal by a resistance network with 2106 components and solved the system of equations. This is the 'true' effective conductivity k_{z_eff}. We compared this value with the upscaled value denoted as $k^{(0)}_{z\_\text{eff}}$. We repeated this calculation for 100 different configurations of the generator with $P = 9$ and $S = 9$. In case of a perfect approximation, the upscaled values must lie on the 1:1 line. The approximated values were distributed close to but systematically below this line and therefore slightly underestimated the true values.

Especially for configurations with low k_{z_eff}-values, the upscaled values $k^{(0)}_{z\_\text{eff}}$ were too low. The larger 'true' conductivity values are caused by the bridging of small particles between separated large particles. This bridging between particles of different sizes is underestimated in the upscaling procedure.
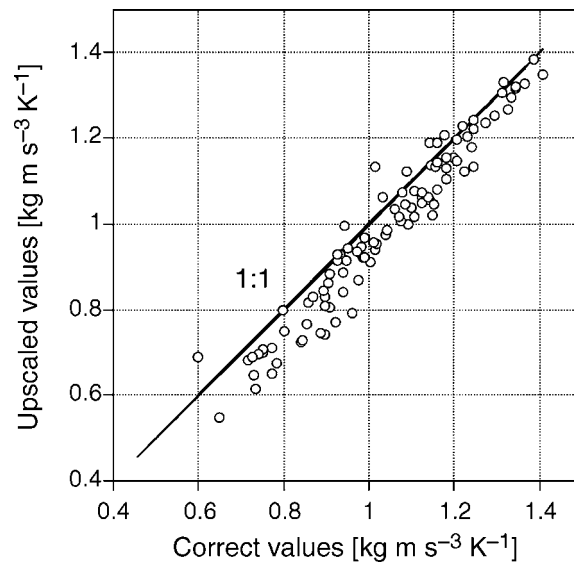

Figure 5. Quality of the upscaling approximation. The approximated values are distributed around the true values (1:1 line). The upscaled values underestimate the true conductivities especially for configurations with low true values.

4.2.4. *Last Step of Upscaling*

After $n-1$ upscaling steps, we have a single structure of size L, which consists of P pores, S solids and F composite structures with size LR^{-1}. The thermal conductivity of the composite structure is characterized by $k^{(1)}_{z\_\text{eff}}$, $k^{(1)}_{y\_\text{eff}}$ and $k^{(1)}_{x\_\text{eff}}$. We solve the flow problem at this scale for a temperature gradient applied in z-direction. The resulting $k^{(0)}_{z\_\text{eff}}$ can be compared with the thermal conductivity of a soil under conditions, where a vertically directed temperature gradient between the atmosphere and the subsoil exists. The upscaled conductivity $k^{(0)}_{z\_\text{eff}}$ depends on the spatial arrangement of pores and particles. We explore this influence in the next subsection.

4.3. INFLUENCE OF SPATIAL ARRANGEMENT

We investigated the influence of the spatial arrangement of the constituents for a generator with $R = 3$, $S = 8$ and $P = 7$. A particular arrangement of pores and particles in a generator is called configuration. We simulated 1000 configurations of the generator. Thereby, we arranged pores and particles randomly and used the same configuration for all the 10 iterations of the prefractal. We assumed air-dry conditions with air-filled pores and conductivity $k_\text{pore} = k_\text{air} = 0.025\,\text{kg m s}^{-3}\,\text{K}^{-1}$. For particles, we chose a conductivity value $k_\text{particle} = 2.9\,\text{kg m s}^{-3}\,\text{K}^{-1}$, typical for the most soil minerals with the exception of quartz. A temperature gradient was imposed in the z-direction and we computed the heat flow and the effective thermal conductivity $k^{(0)}_{z\_\text{eff}}$ in the same direction.

The spatial arrangement of the soil constituents strongly influenced the thermal conductivity of the prefractal. Figure 1 shows four selected configurations corresponding to maximum (1(c)), minimum (1(d)) and average (1(e)) thermal conductivities, respectively.

The largest conductivity value ($1.34\,\text{kg m s}^{-3}\,\text{K}^{-1}$), was found for a configuration with two continuous vertical stacks of particles that linked the bottom and top directly. In case of the minimum conductivity ($0.08\,\text{kg m s}^{-3}\,\text{K}^{-1}$), the particles were surrounded by pores and there was no bridging between particles of different sizes in z-direction. The ratio between the largest and smallest conductivity was 16.75, indicating a substantial influence of the phase topology on thermal conductivity. The mean conductivity, averaged over 1000 realizations, was equal to $0.54\,\text{kg m s}^{-3}\,\text{K}^{-1}$ and the standard deviation was $0.06\,\text{kg m s}^{-3}\,\text{K}^{-1}$. A configuration whose conductivity was equal to the mean is shown in Figure 1(e). In this structure, there is no direct connection between top and bottom through large particles, but top and bottom are linked by the bridging of large and smaller particles. The same is true for the structure presented in Figure 1(b). In the next section, we compute the thermal conductivity of prefractals with partial ice-saturation.

5. Thermal Conductivity of Partially Saturated Soils

With the 3G-PSF approach the pore structure of a soil material can be modeled. Given this structure, we calculate transport properties of soils. With the upscaling

scheme presented in the previous section, we are now armed to predict the thermal conductivity of a soil from its fractal structure.

5.1. FREEZING OF PARTIALLY WATER SATURATED SOILS

In small pores, liquid water may persist at temperatures below the freezing point of free water. The temperature at which water freezes depends on the pore diameter (Miller, 1980). For the remainder of our analysis we assume that the temperature is below the critical value, so the pores are either filled with ice or air. In the unfrozen soil, pore-size and pore-connectivity control which pores are occupied by liquid water for a particular matric potential. To simplify the analysis, we neglect the influence of pore-connectivity and assume that only the pore-size controls the water retention of the fractal soil model. For a particular matric potential head value $|h|$ [m], all the pores of size $LR^{-i} < 4\sigma\, g^{-1} \rho_{water}^{-1} |h|^{-1}$ are filled with water, where σ [kg s^{-2}] is the surface tension of water, ρ [kg m^{-3}] the density and g [m s^{-2}] the gravity acceleration. The factor 4 is a shape factor depending on circumference and cross-section of the water-filled pore (2 for a circle, 4 for a square). On freezing, the volume of water expands and ice partially fills pores of size $LR^{-(i-1)}$. The relative volume occupied by ice in pores of size $LR^{-(i-1)}$ is equal to

$$f_{ice} = \left(\frac{\rho_{water}}{\rho_{ice}} - 1 \right) \frac{\sum_{j=i}^{j=n} p_j}{p_{i-1}},$$

where p_j is the volume of pores with size LR^{-j}. It may happen that $f_{ice} > 1$ and pores of size $LR^{-(i-2)}$ will be partially filled with ice. However, there is only *one* pore-size class that contains both air and ice. First, the edges of the pores become ice-filled and the walls of particles become ice covered. For this class we assume that the ice coats the walls of the pores by a layer of thickness $LR^{-(i-1)} \ell^{-1}$ and an air-filled cube of size $LR^{-(i-1)} (1 - 2\ell^{-1})$ remains in the center of the pore, where ℓ is equal to

$$\ell = \frac{2}{1 - (1 - f_{ice})^{1/3}}.$$

As in the previous section 4.2, we can calculate the effective thermal conductivity of such a composite pore using a resistance network representation and Kirchhoff's laws.

5.2. THERMAL CONDUCTIVITIES OF THE FITTED PREFRACTALS

For each soil we simulated 100 random configurations using the fitted parameters $L, n_1, n_2, S_1, P_1, S_2, P_2, S_3$ and P_3 and we calculated the thermal conductivities for varying ice content θ_{ice} [m^3 m^{-3}], the volume of ice per soil volume. Air-filled pores have a conductivity $k_{air} = 0.025$ kg m s^{-3} K^{-1} and pores completely filled with ice
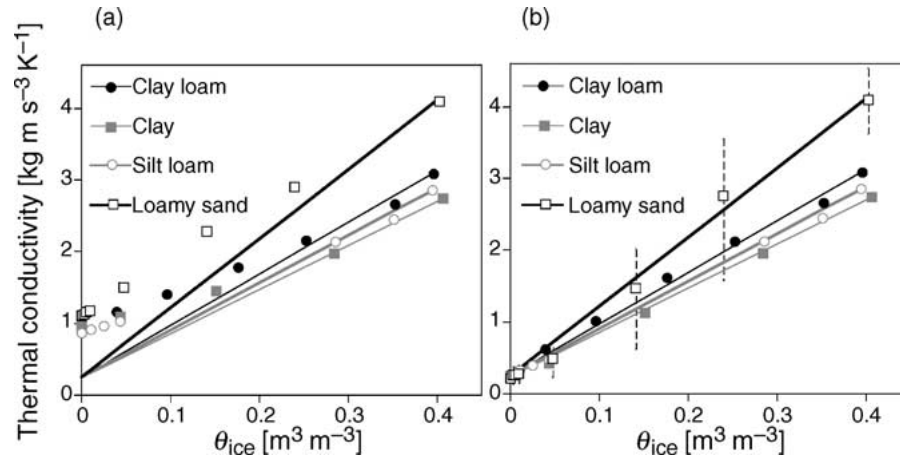
Figure 6. Thermal conductivities of prefractals generated according to the given particle-size distribution (symbols). The lines represent the calculations based on Johansen's approach. In one case (b) the heat transfer of particles is reduced. For the loamy sand, the range of calculated thermal conductivities is shown (dotted vertical lines).

a conductivity of $k_{ice} = 2.2 \, \text{kg m s}^{-3} \, \text{K}^{-1}$. For partially ice-filled pores we computed an effective thermal conductivity. We further assumed that particles larger than 65 μm contain quartz minerals with $k_{quartz} = 7.7 \, \text{kg m s}^{-3} \, \text{K}^{-1}$ while smaller particles contain other minerals with conductivity $k_{mineral} = 2.9 \, \text{kg m s}^{-3} \, \text{K}^{-1}$. Note that for a prefractal of order n only n pore-size classes exist and consequently there are only $n + 1$ values of θ_{ice} for which we predicted the effective thermal conductivity of the prefractal (including the air-dry state). Figure 6(a) shows the effective thermal conductivity of the prefractals (averaged over 100 configurations) in dependence of the ice content. In addition, the figure shows the thermal conductivities as predicted by the empirical approach of Johansen (1975), which is, according to Farouki (1981), the best approach to simulate thermal conductivity. The thermal conductivity of frozen soils depends linearly on the ice content θ_{ice}

$$k(\theta_{ice}) = (k_{sat} - k_{dry})\left(\frac{\theta_{ice}}{\phi}\right) + k_{dry},$$

where k_{sat} and k_{dry} denote the thermal conductivities under saturated and air-dry conditions, respectively. The calculation of these values can be found in the appendix.

Under partially and completely saturated conditions, the effective conductivities predicted by the fractal approach and the Johansen' model, rank in the order of sand fraction:

loamy sand (0.80) ≫ clay loam (0.30) > silt loam (0.15) > clay(0.10).

The number in parentheses denote the sand mass fractions of the four soils. Compared with Johansen's model our approach overpredicts the thermal conductivity

for air-dry conditions. This difference is caused by an overestimated heat exchange between particles. According to Farouki (1966), the contact conduction between particles is the major factor limiting the overall conduction under dry conditions. In our model, we have so far assumed that the entire surface of a solid cube is in contact with the surfaces of adjacent cubes. This is not realistic because solid particles in soils typically have irregular shapes and the contact area between a particle and its neighbors is mostly much smaller than its total surface area. We accounted for the overestimation of contact by the introduction of a reduced heat exchange coefficient k_{boundary} for particles under unsaturated conditions. In the Appendix, we explain a model that can describe this effect of reduced heat exchange. For each value of θ_{ice} we then recomputed the thermal conductivities of the same 100 configurations and calculated their average. For air-dry conditions, the thermal conductivities of all four soils were now very similar (Figure 6(b)) and hence dominated by the contact barrier between the particles. With the fractal model we can also calculate the distribution of thermal conductivity for a certain prefractal and soil. Vertical lines in Figure 6(b) denote the range of the 100 computed values for the loamy sand. The standard deviation is less than 5% but the minimal and maximal values deviate more than 50% from the average for ice content below saturation.

The linear increase of thermal conductivity predicted by the Johansen model is caused by an interplay of two complex mechanisms: while the arrangement of ice and solids in the multiscale structure determines the conductivity for high ice saturations, the reduced contact between particles is dominating for dry conditions.

6. Summary and Conclusions

We presented a fractal approach to model the volumetric distribution and some aspects of the spatial arrangement of the soil constituents.

3G-PSF were fitted to data about porosity and particle-size distributions of four soils (clay, clay loam, silt loam and loamy sand). For all soils the maximum difference between simulated and observed mass fractions was less than 10%. In contrast, a single generator PSF resulted in differences up to 50%. The thermal conductivities of the prefractals were calculated for the same four soils for different ice saturations and were compared with an empirical model well proven in practice. A good agreement between the Johansen' model and the fractal predictions was found. However, for some particular topological arrangement of the soil constituents, deviations from the empiric model are possible. Therefore, some information about the spatial arrangement of pores and solids are needed. In a next step, we will include the connectivity of the pores in the prefractal to calculate the water retention function. For a prefractal fitted according to the measured particle-size distribution and porosity, the computed water retention function for different configurations must be compared with measured water retention data. A prefractal configuration with a water retention function similar to the measured data, models

also the connectivity of the pores and the thermal conductivity can be predicted more precisely.

Appendix

For saturated frozen soils, Johansen (1975) proposed that the thermal conductivity k_{sat} can be predicted by

$$k_{\text{sat}} = k_{\text{quartz}}^{(1-\phi)\,f_{\text{sand}}}\, k_{\text{mineral}}^{(1-\phi)\,(1-f_{\text{sand}})}\, k_{\text{ice}}^{\phi},$$

where f_{sand} is the mass of sand per mass of solid material. We estimated f_{sand} as the mass fraction of particles larger than 65 μm in diameter. To predict the thermal conductivity of the air-dry soil, k_{dry}, Johansen used the semi-empirical equation

$$k_{\text{dry}} = \frac{0.135\rho_{\text{bulk}} + 64.7}{\rho_{\text{particle}} - 0.947\rho_{\text{bulk}}} = \frac{0.135\rho_{\text{particle}}\,(1-\phi) + 64.7}{\rho_{\text{particle}}(0.053 - 0.947\phi)}.$$

We estimated the density of the solid material ρ_{particle} by the corresponding value for quartz sand $\rho_{\text{particle}} = 2650\,\text{kg}\,\text{m}^{-3}$.

Under air-dry conditions, the thermal conductivity k_{dry} is dominated by the reduced heat exchange between particles. To describe this effect with a resistor network, we modified the thermal conductivity of the particles k_{particle} under unsaturated conditions. The heat exchange between particles in air-dry soils occurs across thin water films and touching edges. Heat exchange through the air gaps between particles is negligible. In our model, however, we describe the influence of the air-gaps as a reduced heat exchange of the outer shell of the particles. With such description, we can apply the same approach as used before to calculate the thermal conductivity of partially ice-filled pores: we assume that a particle consists of a core with a thermal conductivity k_{particle} and an outer shell with a reduced thermal conductivity k_{boundary}. For a particle with size LR^{-i}, the thickness of the shell is $(LR^{-i})\ell^{-1}$ and the diameter of the cubic core is equal to $(LR^{-i})(1 - 2\ell^{-1})$. To quantify the thickness of the outer shell, we made the following assumptions: first, the volume of the shell should be small compared to the particle volume. Second, the thermal conductivity of the outer shell k_{boundary} is dominated by the existence of air that reduces the heat exchange. Therefore, we chose the harmonic mean of air and solid conductivity k_{air} and k_{particle} to quantify thermal conductivity of the outer shell

$$k_{\text{boundary}} = \frac{2k_{\text{air}}\,k_{\text{particle}}}{k_{\text{air}} + k_{\text{particle}}} = 0.05\,\text{kg}\,\text{m}\,\text{s}^{-3}\,\text{K}^{-1}.$$

Third, the influence of the air phase has to decrease with increasing water saturation. For a matric potential head $|h|$, pores with size $LR^{-i} < 4\sigma\,\text{g}^{-1}\,\rho_{\text{water}}^{-1}\,|h|^{-1}$ are water filled and particles of this size have no shell with reduced heat exchange. Also in case of bigger particles the heat exchange increases, because the particle surface is in contact with smaller saturated composite structures. We assumed that

the volume of the outer shell decreases with increasing water content θ according to a power-law relationship with exponent α, so the thickness of the layer depends on θ according to

$$\ell(\theta) = \frac{2}{1 - (1 + (2(4 - 6\ell_0 + 3\ell_0^2)(\phi - \theta)^\alpha/(\ell_0^3\theta^\alpha)))^{1/3}},$$

where ℓ_0 characterizes the thickness under air-dry conditions. We tested different values for ℓ_0 and α and computed the effect on thermal conductivity. For $l_0 = 40$ and $\alpha = 5$, the predicted thermal conductivity was in good agreement with the empirical Johansen model. The parameter $\ell_0 = 40$ corresponds to a shell volume of 14.3% related to the total particle volume.

References

Adler, P. M.: 1992, *Porous Media: Geometry and Transport*, Butterworth-Heinemann, Boston.

Bird, N. R. A., Bartoli, F. and Dexter, A. R.: 1996, Water retention models for fractal soil structures, *European Journal of Soil Science* **47**, 1–6.

Bittelli, M., Campbell, G. S. and Flury, M.: 1999, Characterization of particle-size distribution in soils with a fragmentation model, *Soil Science Society of America Journal* **63**, 782–788.

Brooks, R. H. and Corey, A. T.: 1964, Hydraulic properties of porous media, Hydrology Papers, Report No. 3, Colorado State University, Fort Collins, CO.

Clerc, J. P., Giraud, G., Laugier, J. M. and Luck, J. M.: 1990, The electrical conductivity of binary disordered systems, percolation clusters, fractals and related models, *Advances in Physics* **39**, 191–301.

Farouki, O. T.: 1966, Physical properties of granular materials with reference to thermal resistivity, *Highway Research Record* **128**, 25–44.

Farouki, O. T.: 1981, Thermal properties of soils, Cold Regions Research and Engineering Laboratory Monograph 81-1.

Feder, J.: 1988, *Fractals*, Plenum Press, NY.

Gautier, Y. and Noetinger, B.: 1997, Preferential flow-paths detection for heterogeneous reservoirs using a new renormalization technique, *Transport in Porous Media* **26**, 1–23.

Hashin, Z. and Shtrikman, S.: 1962, A variational approach to the theory of the effective magnetic permeability of multiphase materials, *Journal of Applied Physics* **33**, 3125–3131.

Johansen, O.: 1975, Thermal conductivity of soils, PhD Thesis, Trondheim, Norway (Cold Regions Research and Engineering Laboratory Draft Translation 637, 1977).

Mandelbrot, B. B.: 1982, *The Fractal Geometry of Nature*, Freeman and Company, NY.

Mickley, A. S.: 1951, The thermal conductivity of moist soil, *American Institute of Electrical Engineers Transactions* **70**, 1789–1797.

Miller, M. N.: 1969, Bounds for effective electrical, thermal, and magnetic properties of heterogeneous materials, *Journal of Mathematical Physics* **10**, 1988–2004.

Miller, R. D.: 1980, Freezing phenomena in soils, in: D. Hillel (ed.), *Applications of Soil Physics*, Academic Press, NY, 254–299.

Mohanty, S.: 1997, Effect of multiphase fluid saturation on the thermal conductivity of geologic media, *Journal of Physics D: Applied Physics* **30**, L80–L84.

Perfect, E., Kay, B. D. and Rasiah, V.: 1993, Multifractal model for soil aggregate fragmentation, *Soil Science Society of America Journal* **57**, 896–900.

Perrier, E., Bird, N. and Rieu, M.: 1999, Generalizing the fractal model of soil structure: the pore-solid fractal approach, *Geoderma* **88**, 137–164.

Rieu, M. and Sposito, G.: 1991, Fractal fragmentation, soil porosity, and soil water properties: I. Theory, *Soil Science Society of America Journal* **55**, 1231–1238.

Sahimi, M.: 1995, *Flow and Transport in Porous Media and Fractured Rock*, VCH, Weinheim, Germany.

Smith, W. O.: 1942, The thermal conductivity of dry soil, *Soil Science* **53**, 435–459.

Thovert, J. F., Wary, F. and Adler, P. M.: 1990, Thermal conductivity of random media and regular fractals, *Journal of Applied Physics* **68**, 3872–3883.

Tyler, S. W. and Wheatcraft, S. W.: 1990, Fractal processes in soil water retention, *Water Resources Research* **26**, 1047–1054.